Magnetic properties of disordered Ni_3C

Lanping Yue, R. Sabiryanov, E. M. Kirkpatrick,* and Diandra L. Leslie-Pelecky
Department of Physics & Astronomy and Center for Materials Research & Analysis, University of Nebraska-Lincoln, Lincoln, Nebraska 68588-0111
(Received 12 April 2000)

The metastable Ni_3C phase has been produced by mechanically alloying Ni and C. Ni_3C particles of diameter 10 nm are produced after 90 h of mechanical alloying with no evidence of crystalline Ni in x ray or electron diffraction. Linear muffin-tin orbital band-structure calculations show that Ni_3C is not expected to be ferromagnetic due to strong Ni-C hybridization in the ordered alloy; however, the introduction of even small amounts of disorder produces locally Ni-rich regions that can sustain magnetism. Mechanically alloyed Ni_3C is ferromagnetic, with a room-temperature coercivity of 70 Oe and a magnetization of 0.8 emu/g at 5.5 T, although the hysteresis loop is not saturated. The theoretical prediction that interacting locally nickel-rich regions may be responsible for ferromagnetic behavior is supported by the observation of magnetically glassy behavior at low magnetic fields.

I. INTRODUCTION

Mechanical alloying is a unique technique for fabricating disordered and nonequilibrium phases.[1] Locally extreme pressures and temperatures that exist over very short times allow the formation of phases that cannot be fabricated using other techniques. Materials produced by mechanical alloying are often atomically disordered due to the high-energy character of the alloying process. Mechanical milling of initially ferromagnetic alloys produces spin glass[2,3] or cluster-glass[4] behavior via atomic-level disordering and the formation of vacancies, grain boundaries, twins, and other defects. Ni_3C is a metastable phase that is expected to be nonferromagnetic due to strong hybridization between Ni and C orbitals. This paper reports the results of a study to determine whether the introduction of disorder in a nonmagnetic alloy can produce magnetic behavior.

Section II describes the fabrication of Ni_3C by mechanical alloying and Sec. III details the structural properties of the alloy. The magnetic properties of mechanically alloyed Ni_3C are presented in Sec. IV and the theoretical calculations in Sec. V. The discussion of Sec. VI shows that the theoretical calculations and experimental measurements support the picture of a locally disordered alloy with Ni-rich regions that can support a magnetic moment. Conclusions are presented in Sec. VII.

II. FABRICATION OF Ni_3C BY MECHANICAL ALLOYING

Ni_3C can be made by mechanical alloying,[5,6] carbon-ion implantation into nickel,[7] reaction between nickel and amorphous carbon films,[8,9] laser irradiation,[10] and chemical synthesis.[11–13] Ni_3C is metastable at room temperature and decomposes at temperatures above 430 °C.[14–16] The metastability of Ni_3C is attributed to the low maximum solubility of carbon in nickel (2.7 at. % at 1600 K), lack of ionic bonding, and only loose covalent bonding.[9] Ni_3C has a close-packed hexagonal structure and may be described by a hexagonal unit cell with lattice constants of $a_h = 2.682$ Å and $c_h = 4.306$ Å (Ref. 17) or a supercell with $a = \sqrt{3}a_h = 4.553$ Å and $c = 3c_h = 12.92$ Å,[14–16] as shown in Fig. 1. The larger unit cell reflects the regular placement of carbon atoms in one-third of the octahedral interstices. The nickel octahedrons are slightly deformed, with the basal plane bonds being slightly longer than the other bond lengths.[15] The carbon-carbon separation distance is very large, leading to a strong hybridization between carbon and nickel states.

The Ni_3C was handled and processed in an Ar-filled glove box to prevent oxidation. Mechanical alloying was performed in a SPEX 8000 mixer/mill in a tungsten-carbide vial with one ball and a ball-to-mass ratio of one. Elemental

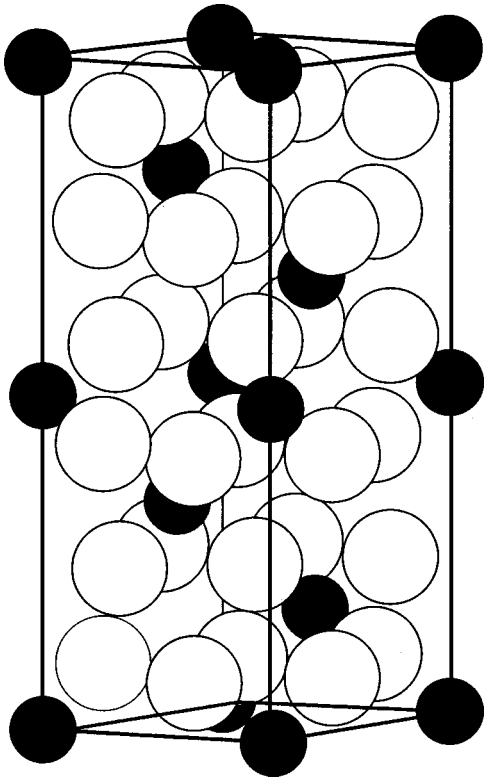

FIG. 1. Crystal structure of Ni_3C.

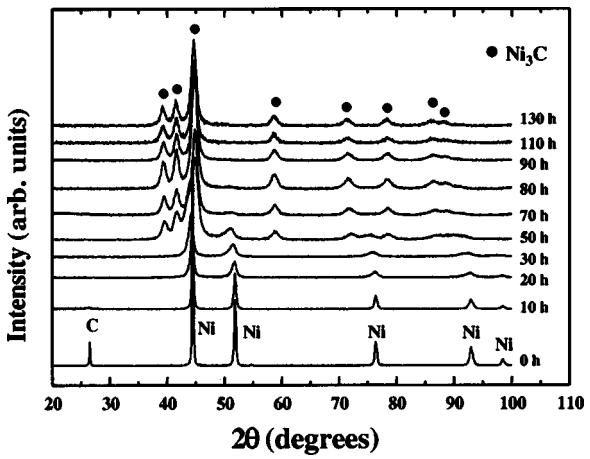

FIG. 2. X-ray-diffraction patterns as functions of mechanical alloying time.

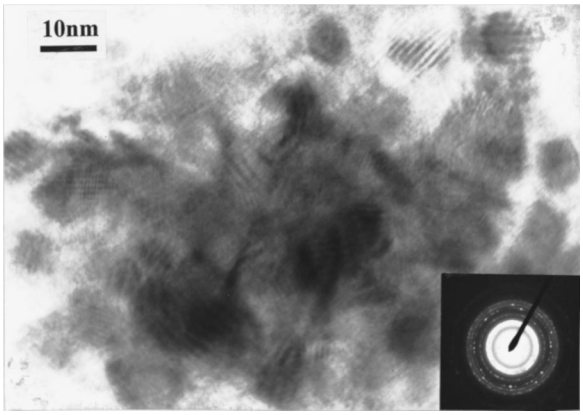

FIG. 4. Transmission electron micrograph of Ni_3C nanoparticles after 90 h of mechanical alloying. The electron-diffraction pattern in the inset shows no evidence of Ni.

graphite (99.5% purity, −325 mesh) and nickel powders (99.9% purity, −325 mesh) were placed in the vial with a slight excess of carbon (3 Ni to 1.05 C), which was necessary to achieve single-phase Ni_3C. The requirement of excess C is attributed to the tendency of the C to coat the milling vial and balls during the early stages of processing. Mechanical alloying was performed in 15-min segments, with a 15-min rest period between segments to limit increases in the vial temperature.

III. STRUCTURAL PROPERTIES

X-ray diffraction was used to monitor the transformation of the Ni-C mixture to Ni_3C. Figure 2 shows the x-ray-diffraction patterns for samples mechanically alloyed for times from 0 to 130 h. The breadth of the diffraction peaks caused overlap in some places, so groups of peaks were separated by fitting to Lorentzian or Pearson VII line shapes. The Scherrer equation[18] was used to extract a diffracting crystallite size (DCS) from the breadth of the K_{α_1} x-ray diffraction line. This value was checked by fitting the data to a single line shape per peak, then numerically correcting for the K_{α_2} contribution using the Rachinger correction.[19] The values from the two methods were consistent with each other to within 10%.

Figure 3 shows the diffracting crystallite sizes of the Ni and Ni_3C extracted from the x-ray diffraction patterns of Fig. 2 as functions of mechanical alloying time. The error bars in Fig. 3 represent the differences between the two methods of calculating the DCS. Figure 2 shows that the peaks due to C disappear entirely after the first 10 h of mechanical alloying. Peaks corresponding to Ni, shown as open circles in Fig. 3, broaden and decrease in intensity and disappear entirely after 90 h of mechanical alloying. Ni_3C peaks, shown as solid squares in Fig. 3, are observed after 50 h of mechanical alloying and indicate a grain size of 9 (±1) nm. The Ni_3C grain size increases slightly with continued mechanical alloying time, reaches a maximum value of 11 (±1) nm after 110 h, and then decreases. Very weak Ni peaks are observed after 170 h of mechanical alloying. The Ni_3C peak positions are uniformly shifted to lower angles with increased mechanical alloying time, suggesting an increased lattice parameter. The maximum shift is 0.4° 2θ after 150 h of mechanical alloying.

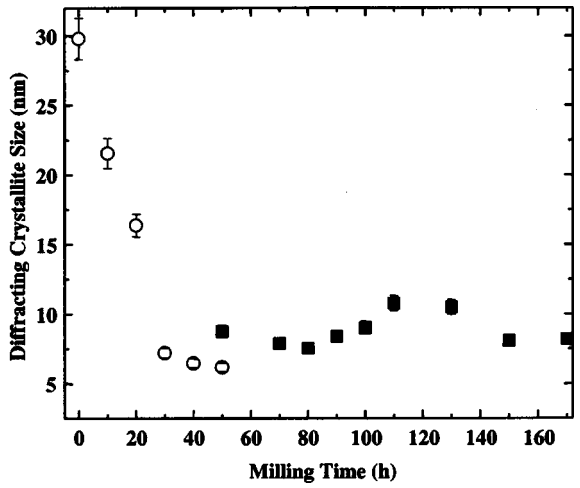

FIG. 3. Diffracting crystallite sizes (DCS) of Ni (open circles) and Ni_3C (squares) from x-ray-diffraction measurements as functions of mechanical alloying time.

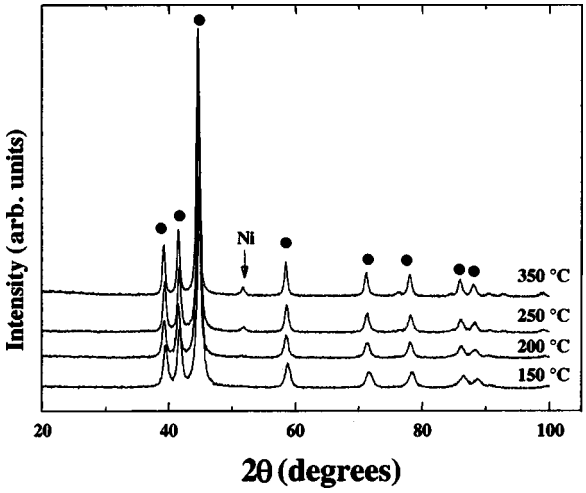

FIG. 5. X-ray-diffraction patterns for samples mechanically alloyed for 90 h, then annealed for 1 h at temperatures from 150 to 350 °C. Solid circles indicate peaks due to Ni_3C.

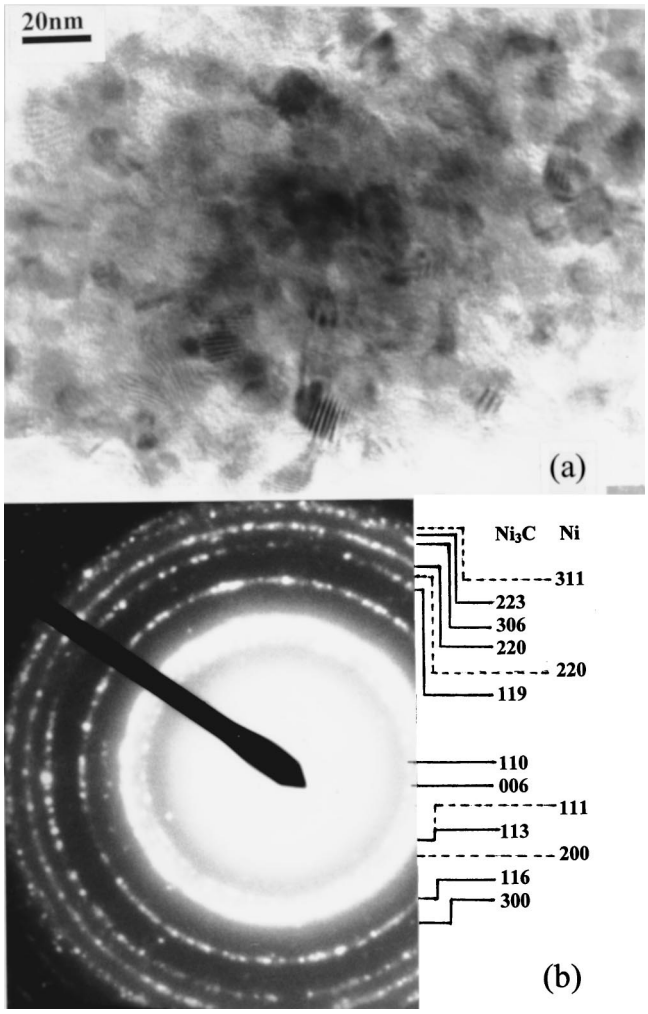

FIG. 6. (a) Transmission electron micrograph of a Ni_3C sample annealed for 1 h at 350 °C. (b) The electron-diffraction pattern shows the presence of Ni and Ni_3C crystallites.

Figure 4 shows a transmission electron micrograph and the corresponding electron diffraction picture of a Ni_3C sample mechanically alloyed for 90 h. The micrograph shows that the Ni_3C particles have an average size of about 10 nm, which is in good agreement with the x-ray-diffraction measurement. The inset shows an electron-diffraction pattern of the same sample. All of the rings in the electron-diffraction pattern can be indexed to the fundamental Ni_3C lines reported by Nagakura;[14,15] however, none of the ''superlattice'' lines observed by Nagakura are observed. We find no evidence of crystalline nickel by electron diffraction or x-ray diffraction.

Figure 5 shows the x-ray-diffraction patterns of Ni_3C samples mechanically alloyed for 90 h, then annealed for 1 h at temperatures from 150 to 350 °C. Ni_3C grain growth is limited at low annealing temperatures; however, the higher annealing temperatures necessary for significant Ni_3C grain growth also produce Ni crystallites. The instability of the Ni_3C phase at higher temperatures is confirmed by transmission electron microscopy [Fig. 6(a)] and electron diffraction [Fig. 6(b)], which show a Ni_3C sample mechanically alloyed for 90 h, then annealed at 350 °C for 1 h. The average diameters of the Ni_3C particles are on the order of 20 nm, which

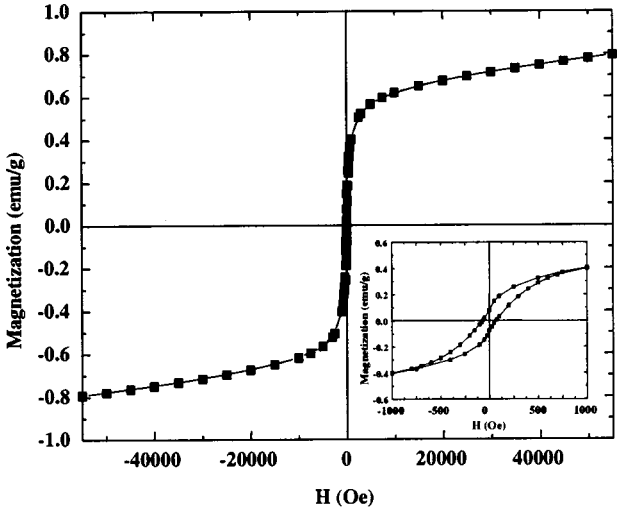

FIG. 7. Room-temperature hysteresis loop showing ferromagnetic behavior. The inset shows the details of the hysteresis loop at low fields.

is again consistent with the DCS values obtained from x-ray diffraction. The electron-diffraction pattern of the same sample shows both Ni_3C and Ni diffraction rings, in contrast to the electron diffraction picture of Fig. 4, which shows only Ni_3C rings.

IV. MAGNETIC PROPERTIES—EXPERIMENTAL RESULTS

Samples for temperature-dependent magnetic measurements were sealed in paraffin-filled polyethylene bags in the Ar atmosphere, or immobilized in vacuum grease in a gelcap. The paraffin was melted to immobilize the powders and prevent motion during measurement. The polyethylene bag or gelcap/grease combination protects the powders from oxidation during the magnetic measurements. Measurements were made in a superconducting quantum interference device with a maximum field of 5.5 T.

Figure 7 shows a room-temperature hysteresis loop for Ni_3C after 90 h of mechanically alloying. The background signal due to the materials used to prevent oxidation is small compared to the sample signal. The sample exhibits ferromagnetic behavior with a coercivity of 70 Oe; however, the hysteresis loop is not saturated at the maximum available field of 5.5 T. The remanence ratio is 0.12 and the magnetization at 5.5 T is 0.8 emu/g.

Figure 8 shows the temperature dependence of the magnetization measured at 5.5 T for the same sample. The data have been corrected for the temperature dependence of the background. The solid line in Fig. 8 shows a fit to a combination of a Bloch law and a Curie–Weiss behavior,

$$M_s(T) = M_o[1 + BT^{3/2}] + \frac{C}{T-\theta} \tag{1}$$

with $M_o = 1.15(\pm 0.01)$ emu/g, $B = -5.6(\pm 0.1) \times 10^{-5}\,\mathrm{K}^{-3/2}$, $C = 11.4(\pm 1.1)$ emu K/g, and $\theta = -34\ (\pm 3)$ K. The value of M_o is significantly less than the bulk

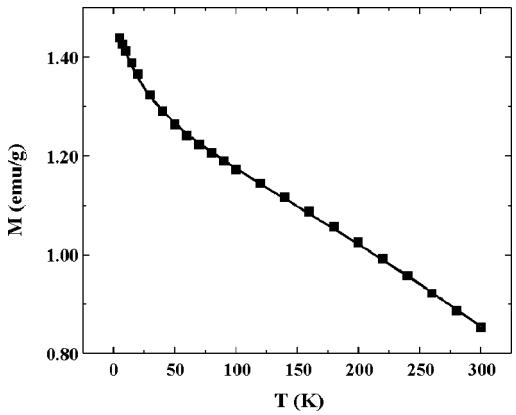

FIG. 8. Temperature dependence of the magnetization at a measuring field of 5.5 T. The solid line is a fit to Eq. (1).

value of M_s for Ni at 4.2 K, which is 58.8 emu/g.[20] The significance of this fit is addressed further in the discussion section.

Figure 9 shows the coercivity and remanence ratio as functions of temperature for a Ni_3C sample mechanically alloyed for 90 h. The coercivity ranges from 70 Oe at room temperature to 600 Oe at 5 K. The coercivity increases more strongly than the $T^{1/2}$ law expected from noninteracting Stoner–Wohlfarth-type particles, but cannot be described by a single power law over the entire temperature range. The remanence ratio ranges from 0.12 at room temperature to 0.43 at 5 K, which is consistent with the presence of demagnetizing interactions.

Figure 10(a) shows the magnetization at 100 Oe as a function of temperature for a Ni_3C sample mechanically alloyed for 90 h. Data were taken in the zero-field-cooled (ZFC) and field-cooled (FC) configurations. The ZFC data show a very broad maximum, with the maximum value of M_{ZFC} occurring at about 220 K. The FC magnetization exhibits irreversibility compared to the ZFC magnetizations at temperatures below the cusp.

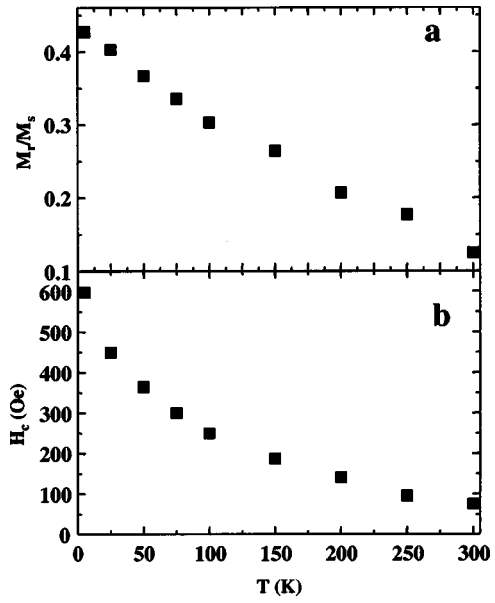

FIG. 9. (a) Remanence ratio and (b) coercivity as functions of temperature for Ni_3C after 90 h of mechanical alloying.

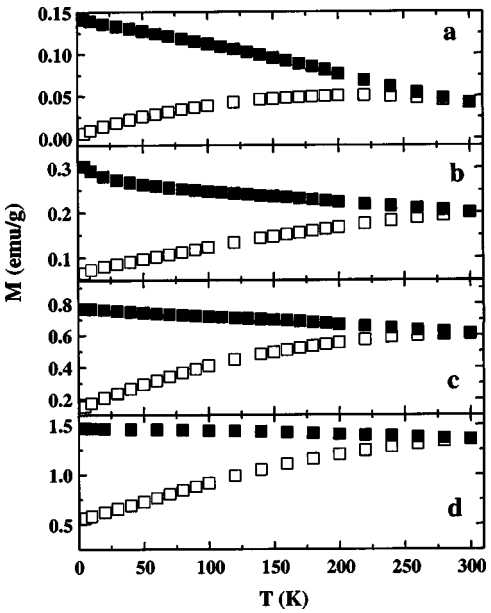

FIG. 10. Field-cooled (solid squares) and zero-field-cooled (open squares) magnetization at 100 Oe for (a) Ni_3C after 90 h of mechanical alloying and the same sample annealed at (b) 200 °C for 1 h, (c) 350 °C for 1 h, and (d) 350 °C for 5 h.

Figures 10(b), 10(c), and 10(d) show the field-cooled and zero-field-cooled magnetizations at 100 Oe for samples annealed at (b) 200 °C for 1 h, (c) 350 °C for 1 h, and (d) 350 °C for 5 h. The same features are observed in the annealed samples as in the unannealed Ni_3C. The overall value of the magnetization increases with annealing temperature and time. The position of the ZFC magnetization maximum is difficult to specify due to limitations on the maximum measuring temperature, but comparison of Figs. 10(a) and 10(b) suggests that the peak shifts to higher temperatures with annealing.

V. MAGNETIC PROPERTIES–THEORY

The electronic band structure of Ni_3C was calculated by the linear-muffin-tin-orbital (LMTO) method. Figure 11(a) shows the density of states (DOS) for ordered Ni_3C. The lowest band is of C *s*-state character. The bottom of the valence band is given by strongly hybridized Ni *p*- and *d*- and C *p* states. The top of the valence band is comprised of mostly Ni 3*d* states, which are highly localized because the large distances between Ni sites limit interaction between neighboring *d* states. The calculations show that the DOS is very small at the Fermi level. The Stoner criterion is not satisfied and Ni_3C is predicted to be nonferromagnetic.

The periodic supercell method was used to remove a carbon site and substitute it with an empty sphere in the LMTO calculations. The DOS for this case is shown in Fig. 11(b), with the solid line showing the DOS for a Ni atom away from the vacancy and the dotted line showing the DOS of the Ni atom closest to the C vacancy. The introduction of the C vacancy removes the hybridization between the Ni and the C

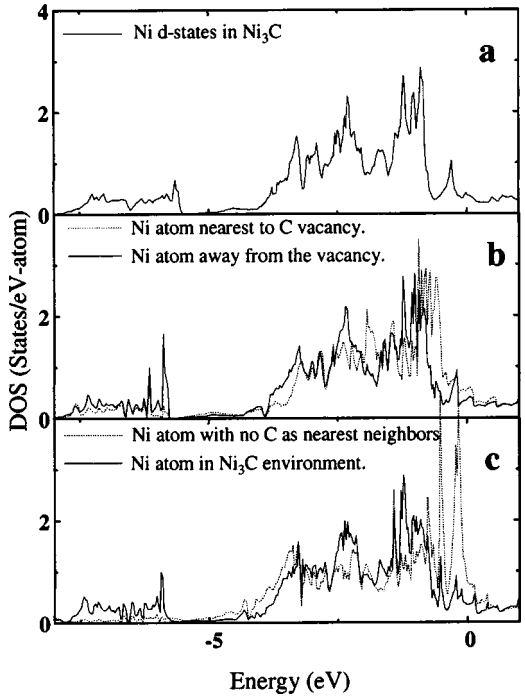

FIG. 11. (a) Density of states for ordered Ni_3C. (b) Density of states for Ni_3C with a C vacancy, with the solid line denoting the DOS for Ni atoms away from the vacancy and the dotted line denoting the DOS for the Ni atom nearest the C vacancy. (c) Density of states for Ni_3C with one plane of C atoms replaced by a plane of Ni atoms. The dashed line shows the DOS for the Ni atom with no C nearest neighbors and the solid line indicates the DOS of the Ni atoms in the Ni_3C environment.

states, which causes an overall shift of the DOS for Ni atoms near the vacancy to higher energy. The DOS near the Fermi level increases, and, although the Stoner criterion is still not satisfied, the compound becomes magnetically unstable.

Figure 11(c) shows the DOS that result if a single C plane is removed and replaced with a Ni plane. The solid line again shows the DOS for a Ni atom in the Ni_3C environment, while the dashed line shows the DOS for a Ni atom with no C nearest neighbors. The region immediately surrounding the defect takes on a stacking pattern very close to fcc Ni. This geometry can be modeled as Ni impurities in the C sites with appropriate relaxation around the impurity. The shift of the DOS for atoms without a nearest C neighbor is even more pronounced, and the main peak in the DOS of the ''Ni-impurity site'' is very close to the Fermi level. The Stoner criterion is close to being satisfied and we expect that this site should be magnetic.

VI. DISCUSSION

The observed ferromagnetic behavior of mechanically alloyed Ni_3C does not agree with the theoretical predictions; however, the observation of ferromagnetic behavior can be explained by disorder in the Ni_3C structure. The magnetic and structural measurements are consistent with a morphology consisting of very small (less than a few nanometers) locally Ni-rich Ni_3C regions of noncompact aggregates that permeate the Ni_3C particles, as illustrated schematically by the cartoon of Fig. 12. This is explicitly *not* a picture of

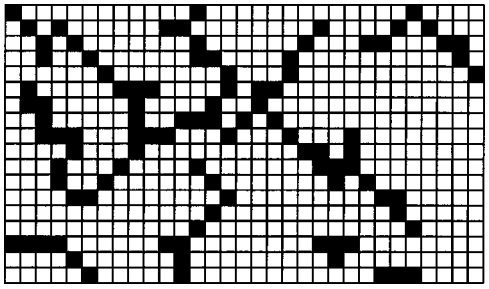

FIG. 12. Cartoon diagram showing the Ni-rich regions in black.

isolated Ni particles in a matrix. A similar picture has been obtained for the Fe-Cu system fabricated by mechanical alloying.[21,22]

The hysteresis loop of Fig. 7 shows ferromagnetic behavior, but is not saturated at 5.5 T, which suggests that there may be some superparamagnetic regions. Superparamagnetic regions could result from parts of the sample that have minimal interactions with other Ni-rich parts. The maximum value of the magnetization is much smaller than is found in Ni nanoparticles, even considering finite size effects.[23,24] The temperature dependence of the maximum magnetization (Fig. 8) shows a combination of a ferromagnetic behavior and a Curie–Weiss behavior, as indicated by the fit to Eq. (1). Some reports suggest that $M_s(T)$ in Ni follows a T^2 behavior in nanostructures[25] and bulk,[26] which is attributed to Stoner-type excitations. Bulk data can be fit using a general treatment of spin-wave interactions,[27,28] which predicts that the next order term is $T^{5/2}$. The Ni_3C data do not require $T^{5/2}$ term for a satisfactory fit; however, the Curie–Weiss behavior may obscure the correction term. Using the T^2 dependence (plus the Curie–Weiss contribution) does not produce a satisfactory fit. The value obtained for parameter B in Eq. (1) cannot be compared to the bulk data because the bulk data require the $T^{3/2}$ and the $T^{5/2}$ terms for a satisfactory fit; however, the value obtained for B is of the correct order of magnitude.

The Curie–Weiss behavior is also consistent with our picture of small, locally Ni-rich interacting regions. Curie–Weiss behavior has been observed in interacting ferrofluids, where θ is a measure of the interaction strength.[29–31] A negative value for θ is attributed to the presence of stronger interactions that cause aggregation and subsequent antiferromagneticlike ordering of the particles. Interactions between Ni-rich regions not in direct contact can occur through the Ni_3C via a Ruderman–Kittel–Kasuya–Yosida-type interaction, which would allow antiferromagnetic interactions.[31]

Annealing decreases the Curie–Weiss contribution to the magnetization at 5.5 T. Samples annealed at 350 °C for 5 h can be fit without the Curie–Weiss contribution, but do require the $T^{3/2}$ and the $T^{5/2}$ terms for an acceptable fit. The parameters obtained from this fit are similar to those of bulk Ni, but with a reduced value of M_o compared to M_s for bulk Ni. This is consistent with part of the sample being nonnickel.

The cusp in the ZFC magnetization (Fig. 10) of a Ni_3C sample mechanically alloyed for 90 h occurs at a high temperature compared to that observed in transition-metal clusters in a nonmagnetic matrix,[17,18] spin glasses,[32] or

ferrofluids.[33] Cusps in the ZFC magnetization can be due to superparamagnetic behavior or to collective behavior of an interacting system, such as in a spin glass.

That crystalline Ni particles are not observed suggests that any nickel particles would be within the size regime where superparamagnetism is expected; however, there is nonzero coercivity below *and* above the cusp temperature. If the cusp is due to superparamagnetism, we can relate the temperature of the maximum in the ZFC magnetization to the product of the anisotropy and the volume as

$$T_B = \frac{KV}{25k_B}, \tag{2}$$

where k_B is the Boltzmann constant. The cusp temperature of 220 K corresponds to $KV = 7.6 \times 10^{-13}$ erg. Five-nm-diameter clusters would thus require an anisotropy of 1.2×10^7 erg/cm^3, which is significantly larger than the bulk Ni value of 6×10^4 erg/cm^3. NiO-coated Ni particles[34] exhibit a cusp in the ZFC magnetization at 220 K, but this is attributable to an enhanced value of K resulting from exchange biasing. The cusp in this case is clearly superparamagnetic, as the coercivity goes to zero in the same temperature range.

The FC data demonstrate significant irreversibility, starting at temperatures as high as room temperature. In contrast to canonical spin glasses, in which the FC data are flat at temperatures below the peak temperature, the FC data here increase almost linearly with decreasing temperature. Similar behavior is seen in frozen ferrofluids[33] and assemblies of nanoparticles,[35] both of which have morphologies similar to that suggested for mechanically alloyed Ni_3C. Annealing increases the temperature of the maximum in the ZFC magnetization to above room temperature, which is consistent with the origin of the maximum in the unannealed sample being small Ni-rich regions. The temperature dependence of the coercivity and the remanence ratio remaining below 0.5 indicate the presence of demagnetizing interactions. The breadth of the maximum is consistent with a broad distribution of interactions, which could be due to lack of uniformity in the distance between Ni-rich regions, or in the size of the regions.

Similar behavior is observed in the $Ni_{80}B_{20}$ system.[36,37] Amorphous Ni-B alloys can be annealed to form crystalline Ni_3B, with no evidence of crystalline Ni. Electron diffraction reveals a very broad ring near the expected position for Ni, which the authors interpret as amorphous or ''noncrystalline'' Ni. Further annealing forms $Ni_3B + Ni$ clusters, similar to our results on annealed Ni_3C. M_s of the noncrystalline Ni phase is 32.9 emu/g, which is about 60% of the bulk value. Our samples were fabricated to have the 3:1 stoichiometry, so the fraction of Ni-rich regions is likely very small compared with the $Ni_{80}B_{20}$ system. The small fraction of Ni-rich regions accounts for the small magnetization values.

The LMTO calculations show that disorder generating as few as three consecutive nickel planes can produce ferromagnetic character in the resulting nickel-rich region. Carbon vacancies, Ni segregation, and extended defects such as dislocations or antiphase boundaries can produce nickel-rich areas. The nature of mechanical alloying is conducive to producing this type of disorder.

The argument may be made that the magnetism in the sample is attributable to unalloyed Ni particles. Although no Ni is observed by x-ray or electron diffraction, it is possible that the fraction of the powder that is Ni is so small that the signal is not observable compared to the signal from the Ni_3C crystallites. The value of the magnetization at 5.5 T in the mechanically alloyed Ni_3C is less than 1 emu/g. If all of the magnetism of the sample is attributed to Ni clusters with the bulk magnetization value of 54.4 emu/g at 300 K,[28] then $\sim$2% of the sample would have to be made up of Ni particles. At this low fraction, the Ni particles would be well separated by the presumably nonmagnetic Ni_3C, and thus be noninteracting. Assuming that the anisotropy is equal to the bulk value for nickel requires that the nickel particles have a particle diameter of 29 nm to account for the position of the cusp in the ZFC magnetization. This value is significantly larger than the mean particle size. The anisotropy can be enhanced in small particles by an order of magnitude,[38] which reduces the particle size necessary to explain the cusp in the ZFC magnetization to a value approximately that of the mean particle size. The noninteracting superparamagnetic picture that this morphology requires, however, is inconsistent with the presence of nonzero coercivity at all temperatures (even above the cusp), and the remanence ratio remaining below 0.5.

VII. CONCLUSIONS

Ni_3C is predicted to be nonmagnetic in the ordered phase. LMTO calculations indicate that even small amounts of disorder bring the system close to satisfying the Stoner criterion via the formation of small, locally Ni-rich regions. We have fabricated Ni_3C by mechanically alloying Ni and C powders. The resulting Ni_3C has an average grain size of 10 nm and exhibits ferromagnetism at all temperatures between 5 and 300 K. The coercivity is 70 Oe at room temperature and rises to 600 Oe at 5 K, while the remanence ratio remains <0.5 for all temperatures. The samples are not saturated at 5.5 T, which suggests that there may be a superparamagnetic component to the magnetization. The temperature dependence of the magnetization indicates the presence of ferromagnetic and Curie–Weiss contributions. These measurements are consistent with a morphology consisting of noncompact Ni-rich regions that permeate the Ni_3C particles. This picture is further supported by the observation of a broad maximum in the zero-field-cooled magnetization, accompanied by irreversibility between the field-cooled and zero-field-cooled magnetizations.

ACKNOWLEDGMENTS

We thank Ralph Skomski, D. J. Sellmyer, R. D. Kirby, and S. S. Jaswal for helpful discussions about this work. The authors acknowledge funding from the National Science Foundation (DMR-9875425 and DMR-9705044) and from the Petroleum Research Foundation, administered by the American Chemical Society.

*Present address: Department of Physics, Rose-Hulman Institute of Technology, Terre Haute, IN 47803.
[1] C. C. Koch, Nanostruct. Mater. **2**, 109 (1993).
[2] G. F. Zhou and H. Bakker, Phys. Rev. Lett. **72**, 2290 (1994).
[3] G. F. Zhou and H. Bakker, Phys. Rev. Lett. **73**, 344 (1994).
[4] E. Bonetti, L. Del Bianco, D. Fiorani, R. Caciuffo, and A. Hernando, Phys. Rev. Lett. **83**, 2829 (1999).
[5] T. Tanaka, K. N. Ishihara, and P. H. Shingu, Metall. Trans. A **23A**, 2431 (1992).
[6] K. Tokomitsu, Mater. Sci. Forum **235–238**, 127 (1997).
[7] J. Wang, X. F. Wu, and B. X. Liu, Acta Metall. Mater. **40**, 1417 (1992).
[8] S. Sinharoy, M. A. Smith, and L. L. Levenson, Surf. Sci. **72**, 710 (1978).
[9] S. Sinharoy and L. L. Levenson, Thin Solid Films **53**, 31 (1978).
[10] V. N. Anisimov, V. Yu. Baranov, L. A. Vladimirtseva, Ch. V. Kopetskii, V. S. Kraposhin, D. D. Malyuta, V. D. Pis'mennyi, A. Yu. Sebrant, and K. V. Shakhlevich, Dokl. Akad. Nauk (SSSR) **286-291**, 866 (1986) [Sov. Phys. Dokl. **31**, 505 (1986)].
[11] Diandra L. Leslie-Pelecky, S.-H. Kim, Michael Bonder, X. Q. Zhang, and Reuben D. Rieke, Chem. Mater. **10**, 164 (1998).
[12] Paul D. Hooker and Kenneth J. Klabunde, Chem. Mater. **5**, 1089 (1993).
[13] Paul Hooker, Beng Jit Tan, Kenneth J. Klabunde, and Steve Suib, Chem. Mater. **3**, 947 (1991).
[14] Sigemaro Nagakura, J. Phys. Soc. Jpn. **12**, 482 (1957).
[15] Sigemaro Nagakura, J. Phys. Soc. Jpn. **13**, 1005 (1958).
[16] R. V. Baranova, Yu. P. Khodyrev, and S. A. Semiletov, Kristallografiya **27**, 923 (1982) [Sov. Phys. Crystallogr. **27**, 554 (1982)].
[17] B. Jacobson and A. Westgren, Z. Phys. Chem. Abt. B **20**, 361 (1933).
[18] P. Scherrer, Gött. Nachr. **2**, 98 (1918).
[19] W. A. Rachinger, J. Sci. Instrum. **25**, 254 (1948).
[20] S. Chikazumi, *Physics of Magnetism* (Wiley, New York, 1964).
[21] A. R. Yavari, P. J. Desré, and T. Benameur, Phys. Rev. Lett. **68**, 2235 (1992).
[22] A. Hernando, P. Crespo, A. García Escorial, and J. M. Barandiarán, Phys. Rev. Lett. **70**, 3521 (1993).
[23] M. J. Aus, B. Szpunar, A. M. El-Sherik, U. Erb, G. Palumbo, and K. T. Aust, Scr. Metall. **27**, 1639 (1992).
[24] J. Ding, T. Tsuzuki, and R. Street, J. Phys. D **29**, 2365 (1996).
[25] H. Kisker, T. Gessmann, R. Würshum, and H. Kronmüller, Nanostruct. Mater. **6**, 925 (1995).
[26] A. T. Aldred, Phys. Rev. B **11**, 2597 (1975).
[27] F. J. Dyson, Phys. Rev. **102**, 1217 (1956).
[28] R. Pauthenet, J. Appl. Phys. **53**, 2029 (1982).
[29] M. Holmes, K. O'Grady, and J. Popplewell, J. Magn. Magn. Mater. **85**, 47 (1990).
[30] F. Söffge and E. Schmidbauer, J. Magn. Magn. Mater. **24**, 54 (1981).
[31] V. M. Dubovik, M. A. Martsenyuk, and N. M. Martsenyuk, J. Magn. Magn. Mater. **150**, 105 (1995).
[32] K. Binder and A. P. Young, Rev. Mod. Phys. **58**, 801 (1986).
[33] Weili Luo, Sidney R. Nagel, T. F. Rosenbaum, and R. E. Rosensweig, Phys. Rev. Lett. **67**, 2721 (1991).
[34] S. Gangopadhyay, G. C. Hadjipanayis, B. Dale, C. M. Sorensen, and K. J. Klabunde, Nanostruct. Mater. **1**, 77 (1992).
[35] K. O'Grady, M. El-Hilo, and R. W. Chantrell, IEEE Trans. Magn. **29**, 2608 (1993).
[36] J. M. Rojo, A. Hernando, M. El Ghannami, A. García-Escorial, M. A. González, R. García-Martínez, and L. Ricciarelli, Phys. Rev. Lett. **76**, 4833 (1996).
[37] C. Ballesteros, A. Zern, A. Garcia-Escorial, A. Hernando, and J. M. Rojo, Phys. Rev. B **58**, 89 (1998).
[38] S. Gangopadhyay, G. C. Hadjipanayis, B. Dale, and C. M. Sorensen, Phys. Rev. B **45**, 9778 (1992).